Journal of Alloys and Compounds 708 (2017) 108–114

Contents lists available at ScienceDirect

Journal of Alloys and Compounds

journal homepage: http://www.elsevier.com/locate/jalcom

Reversible hydrogen storage in $Mg(H_xF_{1-x})_2$ solid solutions

S.A. Pighin [a, b, *], G. Urretavizcaya [a, c], F.J. Castro [a, c]

[a] CNEA, CONICET, Centro Atómico Bariloche, S.C. de Bariloche, Río Negro, Argentina
[b] Universidad Nacional del Comahue, Centro Regional Universitario Bariloche, S.C. de Bariloche, Río Negro, Argentina
[c] Universidad Nacional de Cuyo, Instituto Balseiro, S.C. Bariloche, Río Negro, Argentina

ARTICLE INFO

Article history:
Received 19 December 2016
Received in revised form
22 February 2017
Accepted 27 February 2017
Available online 28 February 2017

Keywords:
Hydrogen storage
Solid solutions
Mechanical milling

ABSTRACT

$Mg(H_xF_{1-x})_2$ solid solutions have been synthesized by mechanical milling MgF_2 and MgH_2 under H_2 atmosphere. Complete solubility has been observed at 475 °C. The solid solution presents a rutile-type structure with the anion site randomly occupied by H^- or F^- and with lattice parameters showing positive deviations from Vegard's law. The solution can be decomposed and re-formed reversibly by changing H_2 pressure. For example, $Mg(H_{0.9}F_{0.1})_2$ reversibly stores 5.5 wt. % H_2 in less than 3 min at 440 °C. During decomposition H_2 is released, and Mg and a solution rich in F appear as products. This process takes place in two clearly marked stages controlled by F^- concentration in the material. The decomposition enthalpy of the first one is close to that of MgH_2 for $Mg(H_{0.9}F_{0.1})_2$, and decreases with the H content in the solution.

1. Introduction

Many binary hydrides are isostructural with the corresponding fluorides. For instance, the alkaline metal hydrides MH (M = Li, Na, K, Rb and Cs) and the fluorides MF share a face-centered cubic structure of the NaCl-type, and among the alkaline – earth metals β-MgH_2 and MgF_2 have the same tetragonal rutile-type structure [1–3]. In this last case, though the hydrides and fluorides of Ca, Sr, Ba are not isostructural, they present similar saline character. Alane and aluminum fluoride are another example of isostructural compounds. These substances have two phases that adopt the same structure: α-AlH_3 and α-AlF_3 (rhombohedral, space group R-3c, 167), and α′-AlH_3 and β-AlF_3 (orthorhombic, space group *Cmcm*, 63) [4,5]. This behavior is mainly due to the similarity between the ionic radii and the electronic configuration of F^- and H^-. The radius of the fluoride ion is 1.33 Å or 1.30 Å with coordination number 6 or 3, respectively [6], whereas that of the hydride ion is in the 1.27 Å – 1.54 Å range [1], depending on the nature of the metal because of its polarizability.

The comparable ionic sizes of both anions allow partial or total substitution of H^- for F^- in hydrides, or *vice versa* in fluorides. For instance, LiH and LiF form solid solutions in the whole range of composition above 321 °C [2], and NaH and NaF also present complete solubility, as has been shown by Majzoub et al. [3], and more recently in a detailed study by Humphries et al. [7]. In the last system the solutions have been prepared by mechanical milling and annealing. In the case of CaF_2, SrF_2 and BaF_2, the fluoride ion can be partially substituted by the hydride ion forming mixed hydride fluorides that keep the fluoride structure. The maximum solubility achieved among these compounds is $CaH_{1.24}F_{0.76}$, $SrH_{0.93}F_{1.07}$ and $BaH_{0.45}F_{1.5}$, clearly showing that solubility decreases with atomic number [8,9]. Substitution has also been observed in ternary hydrides and fluorides, as exemplified by the mixed compounds $XMgH_2F$ and $XMgHF_2$ (X = K, Na) obtained in the systems $XMgF_3$-$XMgH_3$, and the fluorine-substituted complex hydrides $NaBH_2F_2$ and $Na_3AlH_{6-x}F_x$ based on sodium borohydride and sodium alanate, respectively [10–13]. Though the AlH_3-AlF_3 system is related with $Na_3AlH_{6-x}F_x$, no H-F substitution has been experimentally observed in this case. This observation is in agreement with *ab-initio* calculations of a rhombohedral solid solution that give a positive enthalpy of mixing for all values of substitution [14]. The absence of solubility has been attributed to a difference of 22.9% between the cell volumes of AlH_3 and AlF_3, much bigger than the 2.8% observed for Na_3AlH_6 and Na_3AlF_6.

The substitution of H^- by F^- in hydrides has recently received attention due to its potential use in concentrating solar power (CSP) [7,13,15]. Metal hydrides appear as an interesting option as thermochemical heat storage materials thanks to being 5–30 times more energy dense than molten salts, and potentially capable to

* Corresponding author. CNEA, CONICET, Centro Atómico Bariloche, S.C. de Bariloche, Río Negro, Argentina.
E-mail address: spighin@cab.cnea.gov.ar (S.A. Pighin).

http://dx.doi.org/10.1016/j.jallcom.2017.02.297
0925-8388/

operate at temperatures above 600 °C [16]. When used as a thermal storage medium the hydrogen contained in a high-temperature hydride is released using the heat obtained from sunlight and is collected in a low-temperature hydride. The stored heat is recovered by releasing hydrogen from the low-temperature hydride and hydriding the high-temperature hydride. Therefore, the ideal hydride for the high-temperature material is a stable one, capable of absorbing hydrogen at high temperatures and low pressures. For this application the partial substitution of H^- by F^- offers an extra advantage: as metal fluorides are more stable than their equivalent hydrides, a metal-hydrogen-fluorine solid solution is expected to be more stable than the corresponding hydride, and hence, would be capable to operate at a higher temperature without changing the pressure for hydrogen absorption/release.

In this paper we present a study of $Mg(H_xF_{1-x})_2$ solid solutions. As mentioned above, β-MgH_2 and MgF_2 are isostructural, and their cell volumes only differ 5.4%. Though an *ab initio* study of the MgH_2-MgF_2 system has predicted small H solubility in MgF_2 and no F solubility in MgH_2 at room temperature [17], the report of the synthesis of a $MgH_{1.60}F_{0.40}$ solid solution by mechanical milling at room temperature [18] motivates a systematic experimental study of the Mg-H-F system. The results presented here comprise the structural, thermal, and hydrogen storage properties of the $Mg(H_xF_{1-x})_2$ solid solutions. The study is based on samples prepared by mechanically milled MgH_2 and MgF_2.

2. Experimental

The studied materials were prepared by milling commercial MgH_2 and MgF_2 powders (Sigma-Aldrich, 96.5% and 99.9% purity, respectively) in a Fritsch Monomill Pulverisette P6 milling device under 5 bar of H_2 (99.999% of purity) at room temperature. The ball to powder mass ratio used was 40:1, and the milling time was 10 h, in cycles of 10 min of milling followed by 15 min of pause, to prevent overheating. Five compositions were examined corresponding to nominal MgH_2 molar fractions 0.25, 0.375, 0.5, 0.75, and 0.9. The as-milled materials will be hereinafter designated as S0.25, S0.375, etc. Part of the as-milled material was annealed during 16 h under 6 MPa of H_2 pressure at 475 °C to improve homogeneity. These materials will be denoted by codes S0.25A, S0.375A, etc. Additionally, part of the annealed material was remilled 5 h under 5 bar of H_2 to recover the beneficial microstructural characteristics of the milled powders. These materials will be designated by S0.25R, S0.375R, etc.

XRD measurements were done using Panalytical Empyrean and Bruker Advance D8 instruments with Cu Kα radiation. For a precise determination of peak position silicon was used as an internal standard. Rietveld refinement of the diffractograms was done with TOPAS [19]. Hydrogen absorption and desorption were studied at 440 °C and 6 MPa and 10 kPa of H_2 respectively using a custom-made volumetric apparatus [20]. Differential scanning calorimetry (DSC) experiments were performed in DSC 2910 and Q2000, TA Instruments devices, under 122 ml/min Ar flux and 5 °C/min heating rate from 15 to 500 °C. Standard Al pans were used as sample holders. To avoid reactions between Mg and Al (the Al-Mg phase diagram presents two eutectic temperatures at 437 °C and 450 °C [21]), the samples were sandwiched between tantalum films (tantalum films were also used in the reference pan). Thermogravimetry (TG) measurements were performed in a TGA-HP50, TA Instruments, apparatus under 50 ml/min He flux at 5 °C/min heating rate from room temperature to 530 °C. Blank measurements were used as baseline and subtracted from the measured curves. All the handling was done in an Ar-filled glovebox (UNILab-MBraun, O_2 and H_2O levels below 1 ppm).

3. Results and discussion

3.1. Synthesis and structural characterization

The diffractograms of the as-milled materials (Fig. 1) show as main contribution diffraction peaks associated with the MgH_2-MgF_2 mixture. These peaks are located between the reference positions of β-MgH_2 and MgF_2 (ICDD PDF 00-012-0697 and 00-041-1443, respectively) and present different peak shapes and maxima depending on the MgH_2:MgF_2 ratio, as it will be discussed in the next paragraph. Additionally, narrow Si peaks (ICDD PDF 00-026-1481, internal standard) are clearly seen, and small contributions of MgO (ICDD PDF 00-045-0946) and α-Fe (ICDD PDF 03-065-4899) can be observed (unambiguously identified by Rietveld refinement). MgO appears as a reaction product of Mg (impurity of MgH_2) with ambient oxygen during XRD measurement, and the small amount of Fe comes from the milling vessel and balls. Interestingly, only the diffractograms of S0.75 and S0.9 show reflections of γ-MgH_2 (ICDD PDF 00-035-1184). This high-pressure phase usually appears in milled MgH_2 [22], but here it is only observed when the amount of MgF_2 is below the equimolar proportion. It seems that the presence of F above a certain quantity hinders the formation of metastable γ-MgH_2. This result is consistent with the observation of the destabilization of γ-MgH_2 by fluorine [18].

The structural details of the as-milled materials can be better appreciated in Fig. 2a, where an enlarged view of a selected area of the diffractograms is shown. The S0.25 pattern presents two peaks centered on the β-MgH_2 and MgF_2 ICDD card positions. As the MgH_2 content is increased (S0.375) only a single broad peak is observed, with its maximum slightly displaced from the 110 MgF_2 reflection. This shift suggests a change in lattice parameters due to partial H^- solution in the MgF_2 lattice. Besides, peak asymmetry can be attributed to the increased amount of MgH_2 in the material.

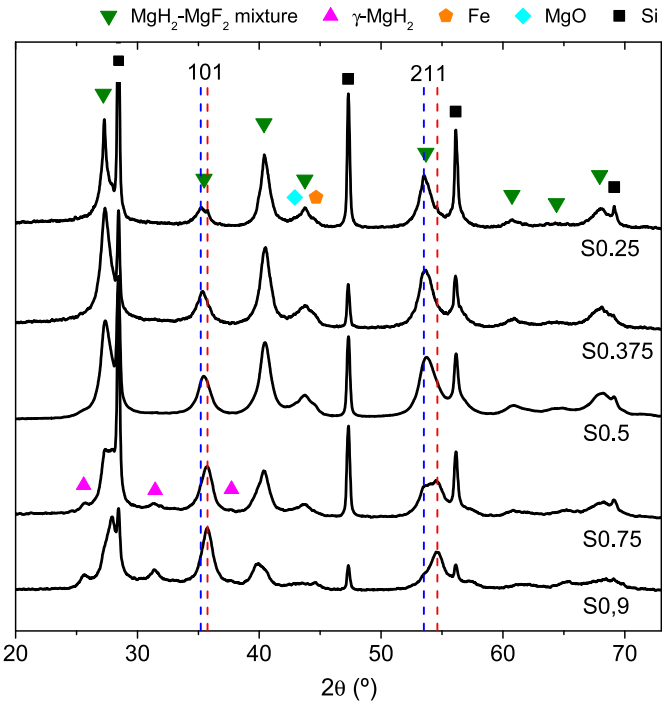

Fig. 1. X-ray diffractograms of the as-milled samples. The positions of reflections 101 and 211 of β-MgH_2 and MgF_2 taken from the corresponding ICDD-PDF files are shown as a reference as red and blue vertical lines, respectively. (For interpretation of the references to colour in this figure legend, the reader is referred to the web version of this article.)

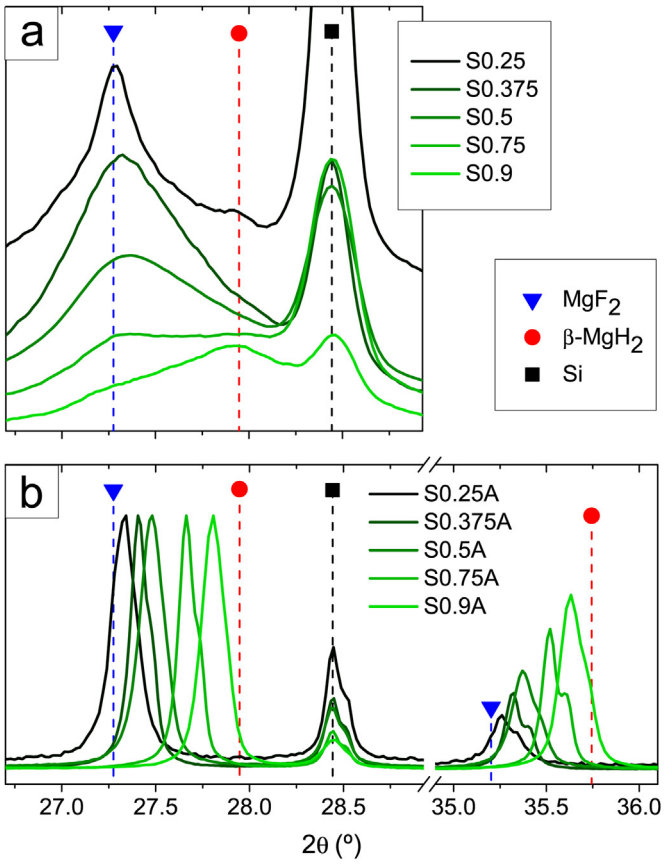

Fig. 2. Detailed view of the X-ray diffractograms of the as-milled (a) and annealed (b) samples.

Sample S0.5 presents a qualitatively similar reflection, with a more noticeable shift in its maximum, compatible with a greater amount of H^- dissolved into MgF_2. With higher MgH_2 proportions (S0.75) the peak changes into an almost flat peak covering the whole range between the 110 β-MgH_2 and MgF_2 reflections. In the richest MgH_2 sample (S0.9) a more pronounced contribution centered on the 110 β-MgH_2 reflection can be seen, though slightly displaced towards lower 2θ angles, indicating that some F^- could be dissolved into MgH_2. The increase in the FWHM of the peak is a consequence of the microstructural modifications induced by milling, together with an important compositional inhomogeneity. If sample S0.5 is milled 5 extra hours, the observed peaks do not significantly change, suggesting that compositional inhomogeneity and microstructure do not vary appreciably with further milling. However, extra milling considerably increases sample contamination with Fe. For this reason, the materials were only milled for 10 h, and homogeneity was obtained by post-milling thermal treatments (samples S0.25A, S0.375A, etc.).

After the heat treatments, the diffraction peaks of the MgH_2-MgF_2 mixture significantly sharpen, and appear between the MgF_2 and β-MgH_2 ICDD locations, with positions strongly correlated with the MgH_2:MgF_2 proportion (Fig. 2b). Peak narrowing is a consequence of homogenization, reduction in defects, residual stress removal and crystallite growth. The location of the peaks suggests that stable solid solutions with the formula $Mg(H_xF_{1-x})_2$ have been obtained. To confirm this hypothesis the diffractograms of the annealed samples were refined using the Rietveld method. The solutions were modeled with a rutile-type $P4_2/mnm$ structure with Mg^{2+} cations filling Wyckoff position 2a and anions occupying Wyckoff position 4f, as suggested by the structure of β-MgH_2 and MgF_2. Disordered solid solutions were assumed, therefore, position 4f has been completely filled with x anions H^- and 1-x anions F^-, the H^- occupancy x treated as a refinable parameter. The refinement also included Si, MgO, Fe and Mg_2FeH_6, this last phase forms in a small amount during the heat treatment under hydrogen pressure. Fig. 3 illustrates a typical refinement of a diffractogram (S0.375A), and Table 1 compiles the refinement results. In all cases the main phase could be refined with the proposed structural model showing fine goodness-of-fit parameters. The other contributions (excluding Si) were present in small amounts. The refined x values are slightly but systematically below the x values deduced from the nominal amounts of MgH_2 and MgF_2. The difference can be attributed to the MgH_2 lost as a consequence of the formation of MgO and Mg_2FeH_6, and the distinct purities of the starting materials.

The refined lattice parameters as a function of solid solution composition are presented in Fig. 4. It can be seen that the values smoothly connect the MgF_2 and β-MgH_2 lattice parameters, and show positive deviations from Vegard's law. The change in lattice parameters is a consequence of the different H^- and F^- sizes. The results can be fitted very well by the quadratic functions:

$$a = 4.622 - 0.060\,x - 0.045\,x^2 \quad (1)$$

$$c = 3.051 - 0.010\,x - 0.020\,x^2 \quad (2)$$

The results presented above show that β-MgH_2 and MgF_2 exhibit complete solubility at 475 °C. This behavior could have been expected because both compounds are isostructural and the anionic size of H^- and F^- deduced from the lattice parameters of β-MgH_2 and MgF_2 (1.27A and 1.30A, respectively) differ only in 2.3%, a value substantially smaller than the maximum size difference of about 15% observed in ionic systems that form complete solid solutions [23]. Regarding the maximum H^- solubility in the fluorides of the alkaline-earth elements, the tendency observed by Brice et al. [8,9] for Ca, Sr and Ba hydrofluorides is followed by the MgH_2-MgF_2 system. The H^- solubility increases with decreasing atomic number and ionic radius: $BaH_{0.45}F_{1.55}$, $SrH_{0.93}F_{1.07}$, $CaH_{1.24}F_{0.76}$, Mg: total.

3.2. Hydrogen desorption and absorption

H_2 desorption from sample S0.9R during decomposition at 440 °C and 10 kPa was observed by isothermal volumetric experiments (Fig. 5). At least 4.6 wt.% of H_2 is released in less than a

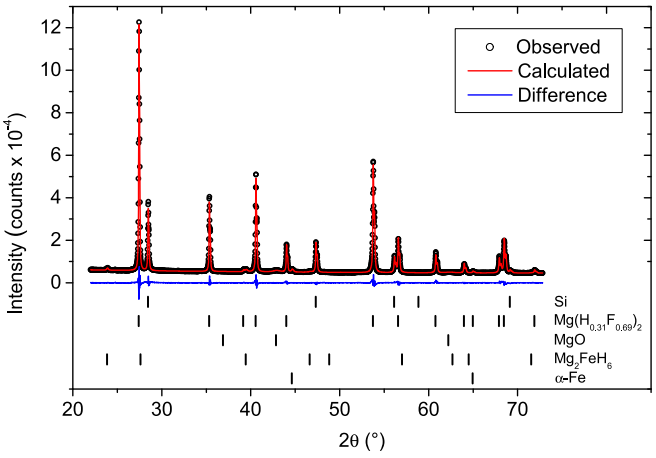

Fig. 3. Example of a Rietveld refinement (S0.375A).

Table 1
Rietveld refinement results of the annealed samples.

Material	x	Cell parameters (Å)		Abundance (wt.%)				R_{exp}	χ^2
		a	c	$Mg(H_xF_{1-x})_2$	MgO	Mg_2FeH_6	Fe		
S0.25A	0.19	4.608(1)	3.048(1)	91	9	<1	<1	2.2	2.3
S0.375A	0.31	4.599(1)	3.046(1)	96	3	<1	<1	2.1	2.3
S0.5A	0.42	4.589(1)	3.043(1)	94	3	2	<1	1.9	2.1
S0.75A	0.70	4.558(1)	3.034(1)	96	3	<1	<1	2.2	2.2
S0.9A	0.86	4.536(1)	3.028(1)	92	7	<1	<1	5.0	1.4

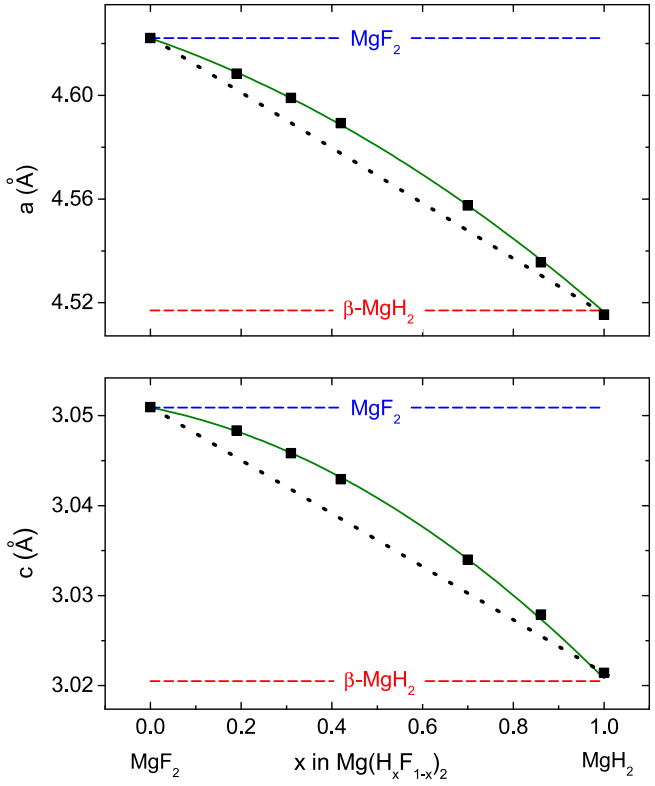

Fig. 4. Lattice parameters of the annealed samples. Error bars are smaller than symbols size. Lattice parameters from ICDD PDF files of β-MgH_2 and MgF_2 (00-012-0697 and 00-041-1443, respectively) are shown as dashed lines. Dotted lines represent Vegard's law.

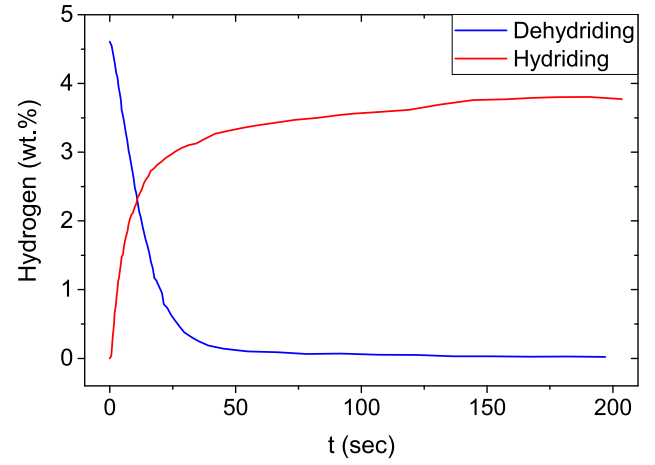

Fig. 5. Isothermal hydriding (6 MPa) and dehydriding (10 kPa) curves of S0.9R at 440 °C.

minute in a single step, without incubation time. The actual amount of H_2 desorbed cannot be determined with accuracy due to the combination of a fast desorption process and an initial blind period of a couple of seconds in the experimental procedure. The XRD diffractogram of the decomposed sample shows Mg as the main phase, together with peaks of a solid solution with low hydrogen content, and residual MgO and Fe (Fig. 6). A detailed view of the solution peaks (see Fig. 6, inset) reveals an asymmetric shape that suggests that instead of a single solution a range of compositions exists in the material. A similar behavior has been observed in the Na-H-F system by Humphries et al. [7]. The overall desorption process can be described by the reaction

$$Mg(H_xF_{1-x})_2\ (s) \rightarrow \frac{1-x}{1-y} Mg(H_yF_{1-y})_2\ (s) + \frac{x-y}{1-y} Mg\ (s) + \frac{x-y}{1-y} H_2\ (g), \quad (3)$$

where a H-rich solution decomposes into a H-poor solution, Mg and H_2. Rietveld refinement of the post-desorption data gives a global y value of 0.2 for the H-poor solution.

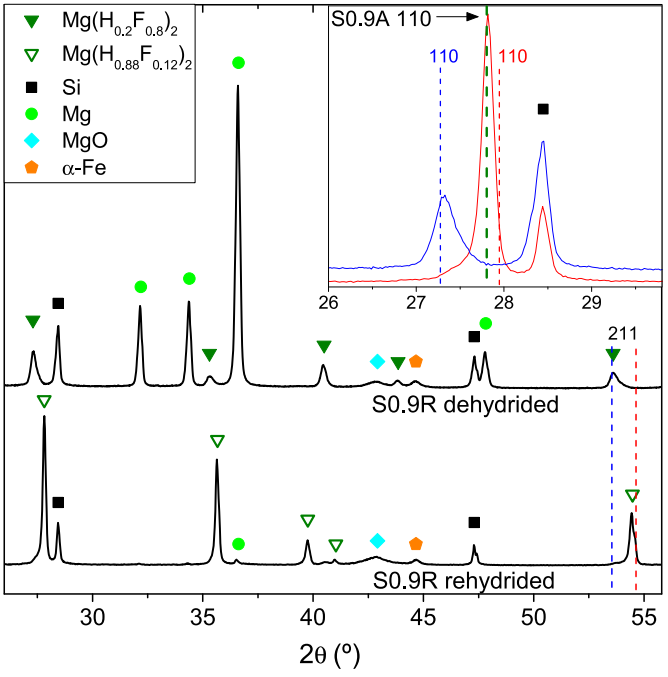

Fig. 6. X-ray diffractograms of dehydrided and rehydrided S0.9R. The positions of reflections 110 and 211 of β-MgH_2 and MgF_2 from the ICDD-PDF files are shown as red and blue vertical lines, respectively. The inset shows an enlarged view of the 110 peak region (rehydrided sample in red and dehydrided one in blue). The dashed vertical line in the inset shows the position of the 110 peak of S0.9A. (For interpretation of the references to colour in this figure legend, the reader is referred to the web version of this article.)

The desorbed solution can be rehydrided at the same temperature by exposing the decomposed sample to 6 MPa of H_2 pressure (Fig. 5). Hydriding also occurs quickly. The material reabsorbs at least 3.8 wt.% in approximately 150 s in a single step. Again, the combination of fast kinetics and the initial blind period hinders the determination of an accurate H content. However, an XRD of the rehydrided sample (Fig. 6) proves that hydrogen absorption has nearly reached completion. The diffractogram presents a solid solution as main contribution, together with residual MgO, Mg and Fe reflections. A closer view of the solution peaks (see Fig. 6 inset) shows that they are composed of a main peak with a small shoulder on its left side. Therefore, the diffractogram was refined including two solutions, one corresponding to a H-rich solution ($Mg(H_{0.88}F_{0.12})_2$, 70 wt.%) and the other to a H-poor solution ($Mg(H_{0.30}F_{0.70})_2$, 5 wt.%). The composition of the H-rich solution closely matches that of the original sample, showing that the system presents good reversibility. The small contribution of the H-poor solution is attributed to partially reacted material. Globally the hydrogen absorption process can be described by the reverse of reaction (3), but the detailed process is not yet clear. One possibility is that H_2 reacts simultaneously with the H-poor solution and Mg to give a H-richer solution, as it has been suggested for the Na-H-F system [7]. Another option is to form MgH_2 from H_2 and Mg first, and then a H-rich solution from the interdiffusion of H^- between MgH_2 and the H-poor solution.

A detailed kinetic study of hydrogen absorption and desorption in this material has not been done yet, but it can be mentioned that at 300 °C kinetics is severely limited. No significant H_2 desorption was registered at this temperature after 2 h at 10 kPa. Despite this, from the point of view of possible applications, the remarkable point is that at least at 440 °C the solid solutions can reversibly release and absorb H_2.

3.3. Thermal analysis

The release of H_2 from the solid solutions during DSC experiments is observed as single endothermic events with decreasing areas only for samples S0.9R, S0.9A, S0.75A and S0.5A (Fig. 7). The DSC runs of the H-poor samples S0.375A and S0.25A do not significantly deviate from the baseline. This behavior is discussed below by combining these results with TG measurements. H_2 release in the annealed materials takes place between 400 °C and 500 °C. The microstructural changes induced by milling reduce these temperatures in almost 100 °C, as can be seen by comparing the thermograms of the remilled S0.9R with that of S0.9A.

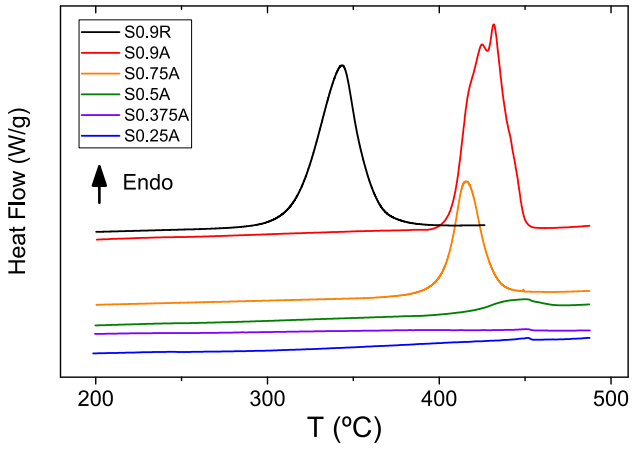

Fig. 7. DSC curves of selected samples.

Interestingly, mass loss during TG measurements occurs in two clearly marked stages: a fast one between 300 °C and 360–370 °C, and a slow one from these temperatures up to 530 °C for the remilled materials (Fig. 8). During the fast stage S0.9R releases 5.5 wt.% of H_2 (Fig. 8a), whereas S0.75R desorbs 2.8 wt.% (Fig. 8b). In the slow stage S0.9R releases 0.4 wt.%, whereas S0.75R desorbs 0.6 wt.%. A similar behavior has been observed in a MgH_2-NbF_5 mixture and has been attributed to different desorption regimes consequence of a F^- blocking effect due to the limited F^- mobility in the lattice [18]. According to this hypothesis, the second regime occurs when the F^- concentration in the product solution of reaction (3) reaches a critical value that severely affects H^- mobility by blocking diffusion sites. From the TG data it can be estimated that the desorption stages are separated by $y = 0.44$ and $y = 0.37$ for S0.9R and S0.75R, respectively, *i.e.* a H^- concentration around $y = 0.4$ can be taken as the critical concentration below which F^- blocking affects desorption. As a reference, multi-component diffusional transport in a cubic lattice with an immobile species is severely limited when the fraction of the mobile component falls below 0.3 [24]. From the point of view of applications, the practical reversible capacity of these materials is that of the fast desorption regime. An estimation of this capacity can be made by calculating the amount of hydrogen released when reaction (3) occurs between a starting solution $Mg(H_xF_{1-x})_2$ and a product solution $Mg(H_{0.4}F_{0.6})_2$ (Fig. 9). It can be seen that, as a consequence of the stoichiometry of reaction (3), practical reversible capacities exceeding 4 wt.% are obtained if $x \geq 0.8$.

Comparing the TG and DSC curves (Fig. 8) it is clear that the DSC

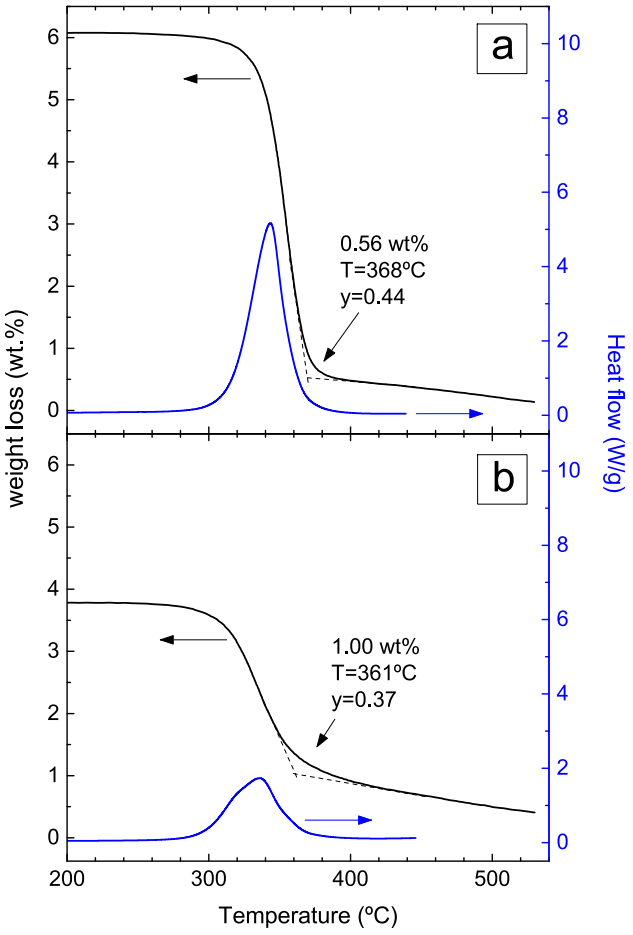

Fig. 8. TG and DSC curves of S0.9R (a) and S0.75R (b).

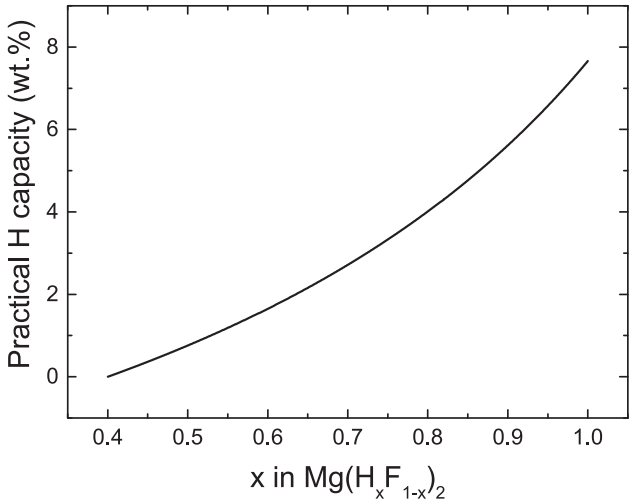

Fig. 9. Practical reversible capacity estimated as the amount of H released when reaction (1) occurs between a starting solution $Mg(H_xF_{1-x})_2$ and a product solution $Mg(H_{0.4}F_{0.6})_2$. Hydrogen content is given as wt.% of the total mass of the sample.

peaks are correlated with the fast desorption regime, whereas no significant thermal events seem to be associated with the slow desorption regime. Usually the heat flow observed in the DSC curves during desorption is proportional to mass loss rate, i.e. the time derivative of the TG curve. This is why a peak is observed in the DSC curve during the fast desorption regime and no significant thermal events are registered during the slow regime. Effectively, the constant heat flow expected in the DSC curve during this last regime cannot be clearly distinguished from the baseline due to the very small mass loss rate associated with this process. Taking into account this explanation it can be understood why the thermograms of S0.375A and S0.25A do not show any thermal events. These samples have an initial H content below the critical concentration, and therefore no fast regime is expected for these materials. Moreover, the existence of a slow desorption regime could be a possible explanation for the difference between the theoretical and observed capacity measured by TPD in the Na-H-F system [7].

From TG and DSC data the decomposition enthalpy associated with the fast regime can be calculated. The values (Table 2) have been obtained by computing the areas under the DSC peaks and determining the amount of H_2 released from the TG data in the temperature range of the fast desorption regime. For higher initial H contents (S0.9A and S0.9R) the ΔH value is around or slightly below 76.1 kJ/mol H_2, the value of MgH_2 [25] (note also that there are not significant differences between the ΔH values of the annealed and remilled materials). For lower initial H contents, the decomposition enthalpy clearly decreases. A similar trend has been observed in the Na-H-F system [7]. This behavior suggests that Mg hydrofluorides could be thermodynamically less stable than MgH_2. However, to fully determine this, the entropic contribution should be known. In the Na-H-F system the decomposition entropy also decreases and the combined enthalpic and entropic effects give an equilibrium pressure for $NaH_{0.5}F_{0.5}$ lower than that of NaH [7], i.e. a more stable material. We expect a similar behavior here, due to a presumed higher entropy of $Mg(H_xF_{1-x})_2$ compared with MgH_2. This higher entropy should produce a lower decomposition entropy that could give a more stable material. However, an in-depth thermodynamic study of this system (currently underway) is needed to ascertain this.

Table 2
Decomposition enthalpy of reaction (3) associated to the fast desorption regime.

Material	ΔH (kJ/mol H_2)
S0.90A	77 ± 5
S0.90R	72 ± 5
S0.75R	65 ± 7
S0.50A	58 ± 11

4. Conclusions

$Mg(H_xF_{1-x})_2$ solid solutions have been obtained by milling MgH_2 and MgF_2 in different proportions. Complete solubility has been observed at 475 °C. The solutions keep the rutile-type structure of β-MgH_2 and MgF_2 with the 4f site randomly occupied by H^- or F^-. The lattice parameters of the structure smoothly connect those of the parent compounds, and exhibit a slight positive deviation from Vegard's law.

The solutions can reversibly release and store H_2. Desorption kinetics comprise a fast desorption regime followed by a slow one. The last one, appears in solutions with x values below 0.4, and is attributed to a desorption process limited by H^- diffusion in a fluoride-blocked lattice. The practically achievable capacity of the H_2-richer mixture is 5.5 wt.% (S0.9R, fast desorption regime). At 440 °C absorption and desorption take less than 3 min.

Decomposition enthalpy at the fast desorption regime is closer to that of MgH_2 for the H-rich solutions, and decreases as the F content of the material increases. Further studies are required to fully characterize the thermodynamic properties of these solid solutions.

Acknowledgements

The authors thank Dr. Julio Andrade Gamboa and Dr. Armando Fernández Guillermet for their valuable comments.

This work was partially supported by grants from Universidad Nacional de Cuyo (06/C417, 06/C486) and CONICET (PIP 112 201101 00524).

References

[1] N.N. Greenwood, A. Earnshaw, Chemistry of the Elements, first ed., Pergamon Press Ltd., Cambridge, 1984.
[2] C.E. Messer, J. Mellor, The system lithium hydride-lithium fluoride, J. Phys. Chem. 64 (4) (1960) 503–505, http://dx.doi.org/10.1021/j100833a507.
[3] E.H. Majzoub, J.L. Herberg, R. Stumpf, S. Spangler, R.S. Maxwell, XRD and NMR investigation of Ti-Compound formation in solution-doping of sodium aluminum hydrides: solubility of Ti in NaAlH4 crystals grown in THF, J. Alloys Compd. 94 (1–2) (2005) 265–270, http://dx.doi.org/10.1016/j.jallcom.2004.10.056.
[4] Crystallography Open Database, http://www.crystallography.net/cod (Accessed 22 February 2017).
[5] J. Graetz, J.J. Reilly, V.A. Yartys, J.P. Maehlen, B.M. Bulychev, V.E. Antonov, B.P. Tarasov, I.E. Gabis, Aluminum hydride as a hydrogen and energy storage material: past, present and future, J. Alloys Compd. 509 (2) (2011) S517–S528, http://dx.doi.org/10.1016/j.jallcom.2010.11.115.
[6] R.D. Shannon, Revised effective ionic radii and systematic studies of interatomic distances in halides and chalcogenides, Acta Crystallogr. Sect. A Cryst. Phys. Diffr. Theor. Gen. Crystallogr. 32 (1976) 751–767, http://dx.doi.org/10.1107/S0567739476001551.
[7] T.D. Humphries, D.A. Sheppard, M.R. Rowles, M.V. Sofianos, C.E. Buckley, Fluoride substitution in sodium hydride for thermal energy storage applications, J. Mater. Chem. A 4 (31) (2016) 12170–12178, http://dx.doi.org/10.1039/C6TA03623F.
[8] J.-F. Brice, A. Courtois, J. Aubry, Preparation de la solution solide hydrurofluoree CaF2–xHx (0 < x ≤ 1,24) etude structurale par diffraction des rayons X et par diffraction des neutrons, J. Solid State Chem. 24 (3–4) (1978) 381–387, http://dx.doi.org/10.1016/0022-4596(78)90030-0.
[9] J.-F. Brice, M. Perrin, R. Leveque, Hydrurofluorures Ioniques MF2–xHx (M = Sr, Ba): synthèse et Étude Structurale Par Diffraction Des Neutrons, J. Solid State Chem. 30 (2) (1979) 183–188, http://dx.doi.org/10.1016/0022-4596(79)90099-9.
[10] A. Bouamrane, C. de Brauer, J.-P. Soulié, J.M. Létoffé, J.P. Bastide, Standard

enthalpies of formation of sodium–magnesium hydride and hydridofluorides NaMgH3, NaMgH2F and NaMgF2H, Thermochim. Acta 326 (1–2) (1999) 37–41, http://dx.doi.org/10.1016/S0040-6031(98)00610-8.
[11] L.H. Rude, U. Filsø, V. D'Anna, A. Spyratou, B. Richter, S. Hino, et al., Hydrogen-fluorine exchange in NaBH4-NaBF4, Phys. Chem. Chem. Phys. 15 (41) (2013) 18185–18194, http://dx.doi.org/10.1039/c3cp52815d.
[12] H.W. Brinks, A. Fossdal, B.C. Hauback, Adjustment of the stability of complex hydrides by anion substitution, J. Phys. Chem. C 112 (14) (2008) 5658–5661, http://dx.doi.org/10.1021/jp7100754.
[13] D.A. Sheppard, C. Corgnale, B. Hardy, T. Motyka, R. Zidan, M. Paskevicius, et al., Hydriding characteristics of NaMgH2F with preliminary technical and cost evaluation of magnesium-based metal hydride materials for concentrating solar power thermal storage, RSC Adv. 4 (51) (2014) 26552–26562, http://dx.doi.org/10.1039/C4RA01682C.
[14] J.E. Fonneløp, M. Corno, H. Grove, E. Pinatel, M.H. Sørby, P. Ugliengo, et al., Experimental and computational investigations on the AlH3/AlF3 system, J. Alloys Compd. 509 (1) (2011) 10–14, http://dx.doi.org/10.1016/j.jallcom.2010.08.147.
[15] D.A. Sheppard, T.D. Humphries, C.E. Buckley, What is old is new again, Mater. Today 18 (8) (2015) 414–415, http://dx.doi.org/10.1016/j.mattod.2015.08.003.
[16] D.A. Sheppard, M. Paskevicius, T.D. Humphries, M. Felderhoff, G. Capurso, J. Bellosta von Colbe, M. Dornheim, T. Klassen, P.A. Ward, J.A. Teprovich, C. Corgnale, R. Zidan, D.M. Grant, C.E. Buckley, Metal hydrides for concentrating solar thermal power energy storage, Appl. Phys. A 122 (2016) 395, http://dx.doi.org/10.1007/s00339-016-9825-0.
[17] M. Baricco, M. Palumbo, E. Pinatel, M. Corno, P. Ugliengo, Thermodynamic database for hydrogen storage materials, Adv. Sci. Technol. 72 (2010) 213–278, http://dx.doi.org/10.4028/www.scientific.net/AST.72.213.
[18] S.A. Pighin, G. Urretavizcaya, F.J. Castro, Study of MgH2 + NbF5 mixtures: formation of MgH2−xFx solid solutions and interaction with hydrogen, Int. J. Hydrogen Energy 40 (13) (2015) 4585–4596, http://dx.doi.org/10.1016/j.ijhydene.2015.01.153.
[19] TOPAS V4: General Profile and Structure Analysis Software for Powder Diffraction Data, User's Manual, Bruker AXS, Karlsruhe, 2008.
[20] G. Meyer, D.S. Rodríguez, F. Castro, G. Fernández, Automatic device for precise characterization of hydride-forming materials, in: Hydrogen Energy Progress XI: Proceedings of the 11th World Hydrogen Energy Conference, International Association for Hydrogen Energy, Stuttgart, 1996.
[21] T.B. Massalski, H. Okamoto, P.R. Subramanian, L. Kacprzak, Binary Alloy Phase Diagrams, second ed., ASM International, Materials Park, 1990.
[22] F. Gennari, F. Castro, G. Urretavizcaya, Hydrogen desorption behavior from magnesium hydrides synthesized by reactive mechanical alloying, J. Alloys Compd. 231 (1) (2001) 46–53, http://dx.doi.org/10.1016/S0925-8388(00)01460-2.
[23] W.D. Kingery, H.K. Bowen, D.R. Uhlmann, Introduction to Ceramics, second ed., Wiley, New York, 1976.
[24] N.E. Benes, H.J.M. Bouwmeester, H. Verweij, Multi-component lattice gas diffusion, Chem. Eng. Sci. 57 (4) (2002) 2673–2678, http://dx.doi.org/10.1016/S0009-2509(02)00154-9.
[25] O. Kubaschewski, C. Alcock, P. Spencer, Materials Thermochemistry, sixth ed., Pergamon Press, Oxford, 1993.